

Measurement of the Near-Threshold $e^+e^- \rightarrow D^{(*)\pm}D^{(*)\mp}$ Cross Section using Initial-State Radiation

G. Pakhlova,¹³ K. Abe,⁸ I. Adachi,⁸ H. Aihara,⁴⁵ D. Anipko,¹ V. Aulchenko,¹ T. Aushev,^{18,13} A. M. Bakich,⁴⁰ V. Balagura,¹³ E. Barberio,²¹ A. Bay,¹⁸ I. Bedny,¹ K. Belous,¹² U. Bitenc,¹⁴ I. Bizjak,¹⁴ S. Blyth,²⁴ A. Bondar,¹ A. Bozek,²⁷ M. Bračko,^{8,20,14} T. E. Browder,⁷ M.-C. Chang,⁴ Y. Chao,²⁶ A. Chen,²⁴ K.-F. Chen,²⁶ W. T. Chen,²⁴ B. G. Cheon,² R. Chistov,¹³ S.-K. Choi,⁶ Y. Choi,³⁹ Y. K. Choi,³⁹ S. Cole,⁴⁰ J. Dalseno,²¹ M. Danilov,¹³ A. Drutskoy,³ S. Eidelman,¹ S. Fratina,¹⁴ N. Gabyshev,¹ T. Gershon,⁸ G. Gokhroo,⁴¹ B. Golob,^{19,14} H. Ha,¹⁶ J. Haba,⁸ K. Hayasaka,²² H. Hayashii,²³ M. Hazumi,⁸ D. Heffernan,³² T. Hokuue,²² Y. Hoshi,⁴³ S. Hou,²⁴ W.-S. Hou,²⁶ T. Iijima,²² K. Ikado,²² A. Imoto,²³ K. Inami,²² A. Ishikawa,⁴⁵ R. Itoh,⁸ M. Iwasaki,⁴⁵ Y. Iwasaki,⁸ H. Kaji,²² J. H. Kang,⁵⁰ P. Kapusta,²⁷ N. Katayama,⁸ T. Kawasaki,²⁹ H. R. Khan,⁴⁶ H. Kichimi,⁸ Y. J. Kim,⁵ K. Kinoshita,³ P. Križan,^{19,14} P. Krokovny,⁸ R. Kulasiri,³ R. Kumar,³³ C. C. Kuo,²⁴ A. Kuzmin,¹ Y.-J. Kwon,⁵⁰ J. Lee,³⁷ M. J. Lee,³⁷ S. E. Lee,³⁷ T. Lesiak,²⁷ S.-W. Lin,²⁶ D. Liventsev,¹³ G. Majumder,⁴¹ F. Mandl,¹¹ T. Matsumoto,⁴⁷ A. Matyja,²⁷ S. McOnie,⁴⁰ T. Medvedeva,¹³ W. Mitaroff,¹¹ H. Miyake,³² H. Miyata,²⁹ Y. Miyazaki,²² R. Mizuk,¹³ E. Nakano,³¹ M. Nakao,⁸ H. Nakazawa,⁸ Z. Natkaniec,²⁷ S. Nishida,⁸ O. Nitoh,⁴⁸ S. Ogawa,⁴² T. Ohshima,²² S. Okuno,¹⁵ S. L. Olsen,⁷ Y. Onuki,³⁵ H. Ozaki,⁸ P. Pakhlov,¹³ H. Park,¹⁷ K. S. Park,³⁹ R. Pestotnik,¹⁴ L. E. Piilonen,⁴⁹ A. Poluektov,¹ Y. Sakai,⁸ N. Satoyama,³⁸ O. Schneider,¹⁸ J. Schümann,²⁵ A. J. Schwartz,³ R. Seidl,^{9,35} K. Senyo,²² M. E. Sevier,²¹ M. Shapkin,¹² H. Shibuya,⁴² B. Shwartz,¹ J. B. Singh,³³ A. Somov,³ N. Soni,³³ S. Stanič,³⁰ M. Starič,¹⁴ H. Stoeck,⁴⁰ S. Y. Suzuki,⁸ F. Takasaki,⁸ K. Tamai,⁸ M. Tanaka,⁸ G. N. Taylor,²¹ Y. Teramoto,³¹ X. C. Tian,³⁴ I. Tikhomirov,¹³ T. Tsuboyama,⁸ T. Tsukamoto,⁸ S. Uehara,⁸ T. Uglov,¹³ K. Ueno,²⁶ S. Uno,⁸ P. Urquijo,²¹ Y. Usov,¹ G. Varner,⁷ S. Villa,¹⁸ C. H. Wang,²⁵ Y. Watanabe,⁴⁶ E. Won,¹⁶ Q. L. Xie,¹⁰ B. D. Yabsley,⁴⁰ A. Yamaguchi,⁴⁴ Y. Yamashita,²⁸ C. C. Zhang,¹⁰ Z. P. Zhang,³⁶ V. Zhilich,¹ and A. Zupanc¹⁴

(Belle Collaboration)

¹*Budker Institute of Nuclear Physics, Novosibirsk*

²*Chonnam National University, Kwangju*

³*University of Cincinnati, Cincinnati, Ohio 45221*

⁴*Department of Physics, Fu Jen Catholic University, Taipei*

⁵*The Graduate University for Advanced Studies, Hayama, Japan*

⁶*Gyeongsang National University, Chinju*

⁷*University of Hawaii, Honolulu, Hawaii 96822*

⁸*High Energy Accelerator Research Organization (KEK), Tsukuba*

⁹*University of Illinois at Urbana-Champaign, Urbana, Illinois 61801*

¹⁰*Institute of High Energy Physics, Chinese Academy of Sciences, Beijing*

¹¹*Institute of High Energy Physics, Vienna*

¹²*Institute of High Energy Physics, Protvino*

¹³*Institute for Theoretical and Experimental Physics, Moscow*

¹⁴*J. Stefan Institute, Ljubljana*

¹⁵*Kanagawa University, Yokohama*

¹⁶*Korea University, Seoul*

¹⁷*Kyungpook National University, Taegu*

¹⁸*Swiss Federal Institute of Technology of Lausanne, EPFL, Lausanne*

¹⁹*University of Ljubljana, Ljubljana*

²⁰*University of Maribor, Maribor*

²¹*University of Melbourne, Victoria*

²²*Nagoya University, Nagoya*

²³*Nara Women's University, Nara*

²⁴*National Central University, Chung-li*

²⁵*National United University, Miao Li*

²⁶*Department of Physics, National Taiwan University, Taipei*

²⁷*H. Niewodniczanski Institute of Nuclear Physics, Krakow*

²⁸*Nippon Dental University, Niigata*

²⁹*Niigata University, Niigata*

³⁰*University of Nova Gorica, Nova Gorica*

³¹*Osaka City University, Osaka*

³²Osaka University, Osaka³³Panjab University, Chandigarh³⁴Peking University, Beijing³⁵RIKEN BNL Research Center, Upton, New York 11973³⁶University of Science and Technology of China, Hefei³⁷Seoul National University, Seoul³⁸Shinshu University, Nagano³⁹Sungkyunkwan University, Suwon⁴⁰University of Sydney, Sydney New South Wales⁴¹Tata Institute of Fundamental Research, Bombay⁴²Toho University, Funabashi⁴³Tohoku Gakuin University, Tagajo⁴⁴Tohoku University, Sendai⁴⁵Department of Physics, University of Tokyo, Tokyo⁴⁶Tokyo Institute of Technology, Tokyo⁴⁷Tokyo Metropolitan University, Tokyo⁴⁸Tokyo University of Agriculture and Technology, Tokyo⁴⁹Virginia Polytechnic Institute and State University, Blacksburg, Virginia 24061⁵⁰Yonsei University, Seoul

(Received 12 January 2007; published 27 February 2007)

We report a measurement of the exclusive $e^+e^- \rightarrow D^{(*)\pm}D^{*\mp}$ cross section as a function of center-of-mass energy near the $D^{(*)\pm}D^{*\mp}$ threshold with initial-state radiation. A partial reconstruction technique is used to increase the efficiency and to suppress background. The analysis is based on a data sample collected with the Belle detector with an integrated luminosity of 547.8 fb^{-1} .

DOI: [10.1103/PhysRevLett.98.092001](https://doi.org/10.1103/PhysRevLett.98.092001)

PACS numbers: 13.66.Bc, 13.87.Fh, 14.40.Gx

Exclusive e^+e^- hadronic cross sections to final states with charm meson pairs are of special interest because they provide information on the spectrum of $J^{\text{PC}} = 1^{--}$ charmonium states above the open-charm threshold, which is poorly understood [1]. The observation of the charmoniumlike $Y(4260)$ state, seen only in $J/\psi\pi\pi(KK)$ final states [2–5], has stimulated renewed interest in this field. Curiously, the $Y(4260)$ peak position is close to a local minimum of the total hadronic cross section [6]. The large branching fraction to $J/\psi\pi\pi$ inferred from the total hadronic cross section is unexpected for a conventional charmonium state with such a large mass and width. In a recent measurement [7] the $e^+e^- \rightarrow D\bar{D}$ cross section is described by known charmonium states without a significant $Y(4260)$ contribution. A study of the production cross section of the charmed meson pairs in this energy range could help clarify this intriguing situation.

In this Letter we report a measurement of exclusive cross sections for $e^+e^- \rightarrow D^{*+}D^{*-}$ and $e^+e^- \rightarrow D^+D^{*-}$ [8] using initial-state radiation (ISR). The data used for this analysis correspond to an integrated luminosity of 547.8 fb^{-1} collected with the Belle detector [9] at the $Y(4S)$ resonance and nearby continuum at the KEKB asymmetric-energy e^+e^- collider [10].

To measure the e^+e^- hadronic cross section at \sqrt{s} smaller than the initial e^+e^- center-of-mass (c.m.) energy ($E_{\text{c.m.}}$) at B factories, ISR can be used [11]. ISR allows a measurement of cross sections in a broad energy range while the high luminosity of the B factories compensates for the suppression associated with the emission of a hard

photon. The selection of $e^+e^- \rightarrow D^{(*)+}D^{*-}\gamma_{\text{ISR}}$ signal events using full reconstruction of both the $D^{(*)+}$ and D^{*-} mesons, plus the γ_{ISR} photon, suffers from low efficiency due to the low $D^{(*)}$ reconstruction efficiencies, small branching fractions, and the low geometrical acceptance for the γ_{ISR} , which tends to be emitted along the beam line. Here, we use a method that achieves higher efficiency by requiring full reconstruction of only one of the $D^{(*)+}$ mesons, the γ_{ISR} , and the slow π_{slow}^- from the other D^{*-} . In this case the spectrum of masses recoiling against the $D^{(*)+}\gamma_{\text{ISR}}$ system:

$$M_{\text{rec}}(D^{(*)+}\gamma_{\text{ISR}}) = \sqrt{(E_{\text{c.m.}} - E_{D^{(*)+}\gamma_{\text{ISR}}})^2 - p_{D^{(*)+}\gamma_{\text{ISR}}}^2} \quad (1)$$

peaks at the D^{*-} mass. Here $E_{D^{(*)+}\gamma_{\text{ISR}}}$ and $p_{D^{(*)+}\gamma_{\text{ISR}}}$ are the c.m. energy and momentum, respectively, of the $D^{(*)+}\gamma_{\text{ISR}}$ combination. This peak is expected to be wide and asymmetric due to the photon energy resolution and higher-order corrections to ISR. From the Monte Carlo (MC) simulation the resolution of this peak is estimated to be $\sim 300 \text{ MeV}/c^2$, which is not sufficient to separate the $D\bar{D}^*$, $D^*\bar{D}^*$, or $D^{(*)\pm}D^{*\mp}\pi$ final states. To disentangle the contributions from these final states and to suppress combinatorial backgrounds, we use the slow pion from the unreconstructed D^{*-} . The difference between the mass recoiling against $D^{(*)+}\gamma_{\text{ISR}}$ and $D^{(*)+}\pi_{\text{slow}}^-\gamma_{\text{ISR}}$ (recoil mass difference):

$$\Delta M_{\text{rec}} = M_{\text{rec}}(D^{(*)+}\gamma_{\text{ISR}}) - M_{\text{rec}}(D^{(*)+}\pi_{\text{slow}}^-\gamma_{\text{ISR}}), \quad (2)$$

has a narrow distribution ($\sigma \sim 1.4 \text{ MeV}/c^2$) around the nominal $m_{D^{*+}} - m_{D^{*0}}$, since the uncertainty in γ_{ISR} momentum partially cancels out.

For the measurement of the exclusive cross section, one needs to determine the $D^{(*)+}D^{*-}$ mass when one of the D^{*} 's is not reconstructed. In the absence of higher-order QED processes, $M(D^{(*)+}D^{*-})$ is the mass recoiling against the γ_{ISR} . However, the photon energy resolution results in a typical $M_{\text{rec}}(\gamma_{\text{ISR}})$ resolution of $\sim 100 \text{ MeV}$, which is too wide for the study of relatively narrow $D^{(*)+}D^{*-}$ mass states. We significantly improve the $M_{\text{rec}}(\gamma_{\text{ISR}})$ resolution by applying a refit that constrains $M_{\text{rec}}(D^{(*)+}\gamma_{\text{ISR}})$ to the nominal D^{*-} mass. In this way we use the well-measured properties of the fully reconstructed $D^{(*)+}$ to correct the energy of the γ_{ISR} . As a result, the $M_{D^{(*)\pm}D^{*\mp}} [\equiv M_{\text{rec}}(\gamma_{\text{ISR}})]$ resolution is improved by a factor of ~ 10 and varies from $\sim 6 \text{ MeV}/c^2$ around threshold to $\sim 12 \text{ MeV}/c^2$ at $M_{D^{(*)+}D^{*-}} = 5.0 \text{ GeV}/c^2$. The recoil mass difference after the refit procedure ($\Delta M_{\text{rec}}^{\text{fit}}$) has a resolution improved by a factor of ~ 2 . Finally, the cross section is derived from the $D^{(*)+}D^{*-}$ mass spectrum after the refit.

All charged tracks should originate from the interaction point (IP) with the requirements $dr < 2 \text{ cm}$ and $dz < 4 \text{ cm}$, where dr and dz are the impact parameters perpendicular to and along the beam direction with respect to the IP. Charged kaons are required to have the ratio of particle identification likelihoods, $\mathcal{P}_K = \mathcal{L}_K / (\mathcal{L}_K + \mathcal{L}_\pi)$ [12], larger than 0.6. No identification requirements are applied for pion candidates. K_S^0 candidates are reconstructed by combining $\pi^+\pi^-$ pairs with an invariant mass within $10 \text{ MeV}/c^2$ of the nominal K_S^0 mass. The distance between the two pion tracks at the K_S^0 vertex must be less than 1 cm, the transverse flight distance from the interaction point is required to be greater than 0.1 cm, and the angle between the K_S^0 momentum direction and the flight direction in the x - y plane should be smaller than 0.1 rad. Photons are reconstructed in the electromagnetic calorimeter as showers with energies greater than 50 MeV that are not associated with charged tracks. ISR photon candidates are required to have energies greater than 2.5 GeV. Pairs of photons are combined to form π^0 candidates. If the mass of a $\gamma\gamma$ pair lies within $15 \text{ MeV}/c^2$ of the nominal π^0 mass, the pair is fit with a π^0 mass constraint and considered as a π^0 candidate. D^0 candidates are reconstructed using five decay modes: $K^-\pi^+$, K^-K^+ , $K^-\pi^-\pi^+\pi^+$, $K_S^0\pi^+\pi^-$, and $K^-\pi^+\pi^0$. A $\pm 15 \text{ MeV}/c^2$ mass window is used for all modes except for $K^-\pi^-\pi^+\pi^+$, where a $\pm 10 \text{ MeV}/c^2$ requirement is applied ($\sim 2.5\sigma$ in each case). D^+ candidates are reconstructed using the decay modes $K_S^0\pi^+$, $K^-\pi^+\pi^+$, and $K^-K^+\pi^+$. A $\pm 10 \text{ MeV}/c^2$ mass window is used for all D^+ modes. To improve the momentum resolution of D meson candidates, final tracks are fitted to a common vertex applying the nominal D^0 or D^+ mass as a constraint. D^* candidates are selected via $D^{*+} \rightarrow D^0\pi^+$ and $D^{*0} \rightarrow D^0\pi^0$ decay modes with a

$\pm 2 \text{ MeV}/c^2$ $D^* - D$ mass-difference window. A mass- and vertex-constrained fit is also applied to D^* candidates.

The distribution of $M_{\text{rec}}(D^{*+}\gamma_{\text{ISR}})$ in the data, without any requirements on the slow pion, is shown in Fig. 1(a). The excess around the D^{*-} mass includes the $e^+e^- \rightarrow D^{*+}D^{*-}\gamma_{\text{ISR}}$ signal as well as contributions from the $e^+e^- \rightarrow D^+D^{*-}\gamma_{\text{ISR}}$ channel. The shoulder at higher masses is due to $e^+e^- \rightarrow D^{*+}D^{(*)}\pi\gamma_{\text{ISR}}$. The excess that is evident at $\sim 2.5 \text{ GeV}/c^2$ corresponds to $e^+e^- \rightarrow D^{*+}D^{*-}\gamma_{\text{ISR}}$. The background from the other processes is substantially suppressed by the inclusion of the slow pion from the unreconstructed D^{*-} and the tight requirement on $\Delta M_{\text{rec}}^{\text{fit}}$; i.e., within $\pm 2 \text{ MeV}/c^2$ of the nominal $m_{D^{*-}} - m_{D^0}$, a clean peak corresponding to $e^+e^- \rightarrow D^{*+}D^{*-}$ is evident in the $M_{\text{rec}}(D^{*+}\gamma_{\text{ISR}})$ distribution [Fig. 1(b)]. We define the signal region by the requirement that $M_{\text{rec}}(D^{*+}\gamma_{\text{ISR}})$ be within $\pm 0.2 \text{ GeV}/c^2$ of the nominal D^{*-} mass. This tight requirement suppresses $e^+e^- \rightarrow D^{*+}D^{*-}\pi^0\gamma_{\text{ISR}}$ events, which have a similar $\Delta M_{\text{rec}}^{\text{fit}}$ distribution. The spectrum of $\Delta M_{\text{rec}}^{\text{fit}}$ for the signal $M_{\text{rec}}(D^{*+}\gamma_{\text{ISR}})$ window after the refit procedure in data is shown in Fig. 1(c).

In case of multiple entries, the $D^{*+}\pi$ candidate with the minimum value of $\chi_{\text{tot}}^2 = \chi_{M(D^0)}^2 + \chi_{M(D^{*+})}^2 + \chi_{\Delta M_{\text{rec}}^{\text{fit}}}^2$ is chosen, where each χ^2 is defined as the squared ratio of the

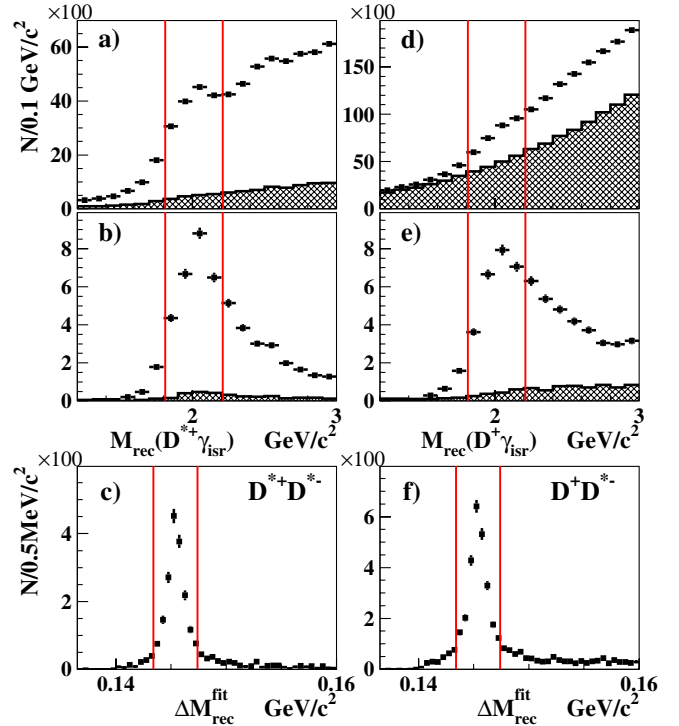


FIG. 1 (color online). The $M_{\text{rec}}(D^{*+}\gamma_{\text{ISR}})$ distribution for the data: (a),(d) without requirement of slow pion; (b),(e) with $\Delta M_{\text{rec}}^{\text{fit}}$ requirement. Histograms show the normalized $M_{D^{(*)+}}$ sidebands contributions. (c),(f) The distribution of $\Delta M_{\text{rec}}^{\text{fit}}$ in the data after the refit procedure. The selected signal windows are indicated by the vertical lines.

deviation of the measured parameter from the expected signal value and the corresponding resolution.

The following sources of background are considered: (1) combinatorial background under the reconstructed D^{*+} peak; (2) real D^{*+} mesons coming from the signal or other processes combined with a combinatorial slow pion; (3) both the D^{*+} and slow pion are combinatorial; (4) the reflection from the process $e^+e^- \rightarrow D^{*+}D^{*-}\pi_{\text{miss}}^0\gamma_{\text{ISR}}$ with an extra π^0 in the final state; (5) the contribution of $e^+e^- \rightarrow D^{*+}D^{*-}\pi^0$ when an energetic π^0 is misidentified as a single γ_{ISR} . The contributions of backgrounds (1) and (2) are extracted using D^{*+} and $\Delta M_{\text{rec}}^{\text{fit}}$ sidebands, which have twice the area of the signal region. The latter sideband is shifted by 10 MeV/ c^2 from the signal region to avoid signal oversubtraction due to the higher-order ISR tail. Background (3) is present in both the $M(D^{*+})$ and $\Delta M_{\text{rec}}^{\text{fit}}$ sidebands and is, thus, subtracted twice. To account for this oversubtraction we use a two-dimensional sideband region, where events are selected from both the D^{*+} and the $\Delta M_{\text{rec}}^{\text{fit}}$ sidebands. The total fraction of backgrounds (1)–(3), found to be as large as $\sim 10\%$, is subtracted from the signal-region $D^{*+}D^{*-}$ mass spectrum. Process (4) produces a broad peak in the $\Delta M_{\text{rec}}^{\text{fit}}$ distribution around the nominal $m_{D^{*-}} - m_{D^0}$ value and, thus, is not contained in the $\Delta M_{\text{rec}}^{\text{fit}}$ sidebands. The dominant part of this background is suppressed by the tight requirement on $M_{\text{rec}}(D^{*+}\gamma_{\text{ISR}})$. The remaining part is estimated by applying a similar partial reconstruction method to the isospin-conjugate process $e^+e^- \rightarrow D^{*0}D^{*-}\pi_{\text{miss}}^+\gamma_{\text{ISR}}$: a D^{*0} is fully reconstructed and the slow pion from a D^{*-} is used for the $\Delta M_{\text{rec}}^{\text{fit}}$ requirement. Since there is a charge imbalance in this final state, only events with a missing extra π_{miss}^+ can contribute to the $\Delta M_{\text{rec}}^{\text{fit}}$ peak. To extract the level of background (4), this spectrum is rescaled according to the ratio of D^{*0} and D^{*+} reconstruction efficiencies and an isospin factor of $\frac{1}{2}$. The contribution from background (4) is found to be consistent with zero. Uncertainties in this estimate are included in the systematic error. The contribution of background (5) is determined from reconstructed $e^+e^- \rightarrow D^{*+}D^{*-}\pi^0$ events using a similar partial reconstruction technique but with an energetic π^0 replacing the γ_{ISR} . The contribution of this background is found to be negligibly small; uncertainties in this estimate are also included in the systematic error.

The analysis of the $e^+e^- \rightarrow D^+D^{*-}$ cross section is identical to that described above for $e^+e^- \rightarrow D^{*+}D^{*-}$ with the fully reconstructed D^{*+} meson replaced by a fully reconstructed D^+ meson. The distribution of $M_{\text{rec}}(D^+\gamma_{\text{ISR}})$ with no requirements on the slow pion from the D^{*-} is shown in Fig. 1(d). The excess around the nominal D^{*-} mass corresponds to the $e^+e^- \rightarrow D^+D^{*-}\gamma_{\text{ISR}}$ signal plus overlaps from the $e^+e^- \rightarrow D^{*+}D^{*-}\gamma_{\text{ISR}}$ channel. The shoulder at higher masses is due to $e^+e^- \rightarrow D^{(*)+}D^{*-}\pi\gamma_{\text{ISR}}$. The requirement of a detected slow pion from the unreconstructed D^{*-} and a tight requirement on

$\Delta M_{\text{rec}}^{\text{fit}}$ provides the clean $e^+e^- \rightarrow D^+D^{*-}$ signal peak in the distribution of $M_{\text{rec}}(D^+\gamma_{\text{ISR}})$ that is shown in Fig. 1(e). The $\Delta M_{\text{rec}}^{\text{fit}}$ distribution for the signal $M_{\text{rec}}(D^+\gamma_{\text{ISR}})$ window is shown in Fig. 1(f). In the case of multiple entries, we apply a single candidate selection procedure similar to that used for $D^{*+}D^{*-}$ to all the distributions shown below.

Similar sources of background (1)–(5) are considered for the $e^+e^- \rightarrow D^+D^{*-}$ study. The contributions of backgrounds (1)–(3) are determined using D^+ and $\Delta M_{\text{rec}}^{\text{fit}}$ sidebands with twice the area of the signal region. Here again, background (3) is present in both $M(D^+)$ and $\Delta M_{\text{rec}}^{\text{fit}}$ sidebands and thus subtracted twice. To account for this oversubtraction we use a two-dimensional sideband region that contains pure background (3) events. The level of contamination from background (4) is determined from isospin-conjugate events, $e^+e^- \rightarrow D^0D^{*-}\pi_{\text{miss}}^+\gamma_{\text{ISR}}$, in the data. The D^+D^{*-} analysis is repeated with the fully reconstructed D^+ 's replaced by fully reconstructed D^0 's. The D^0D^{*-} mass distribution, after combinatorial background subtraction, is rescaled according to the ratio of D^+ and D^0 reconstruction efficiencies and an isospin factor of $\frac{1}{2}$. By chance, the contamination from the process $e^+e^- \rightarrow D^{*+}D^{*-}$, followed by $D^{*+} \rightarrow D^+\pi^0$ is also included in our estimate with correct scaling because $\mathcal{B}(D^{*+} \rightarrow D^+\pi^0)/\mathcal{B}(D^{*+} \rightarrow D^0\pi^+)$ is also $\sim \frac{1}{2}$. The contribution from background (5) determined from reconstructed $e^+e^- \rightarrow D^+D^{*-}\pi^0$ events in the data is found to be negligibly small and taken into account in the systematic error. The total background level is $\sim 20\%$ or less of the signal for all values of $M(D^+D^{*-})$.

The $e^+e^- \rightarrow D^{(*)+}D^{*-}$ cross sections are extracted from the $D^{(*)+}D^{*-}$ mass distributions [13]

$$\sigma(e^+e^- \rightarrow D^{(*)+}D^{*-}) = \frac{dN/dm}{\eta_{\text{tot}}dL/dm}, \quad (3)$$

where $m \equiv M(D^{(*)+}D^{*-})$, dN/dm is the mass spectra obtained before corrections for resolution and higher-order radiation, while η_{tot} is the total efficiency. The factor dL/dm is the differential ISR luminosity

$$dL/dm = \frac{\alpha}{\pi x} \left((2 - 2x + x^2) \ln \frac{1+C}{1-C} - x^2 C \right) \frac{2m\mathcal{L}}{E_{\text{c.m.}}^2}, \quad (4)$$

where $x = 1 - m^2/E_{\text{c.m.}}^2$, \mathcal{L} is the total integrated luminosity, and $C = \cos\theta_0$, where θ_0 defines the polar angle range for γ_{ISR} in the e^+e^- c.m. frame: $\theta_0 < \theta_{\gamma_{\text{ISR}}} < 180 - \theta_0$. The reconstruction efficiencies, determined as a function of $M(D^{(*)+}D^{*-})$ by MC simulation, are found to be independent of $M(D^{(*)+}D^{*-})$ for both processes and are equal to $\eta(D^{*+}D^{*-}) = 4.3 \times 10^{-3}$ and $\eta(D^+D^{*-}) = 3.9 \times 10^{-3}$. The resulting exclusive $e^+e^- \rightarrow D^{(*)+}D^{*-}$ cross sections are shown in Fig. 2 with statistical uncertainties only. Since the bin width is much larger than the resolution, no correction for resolution is applied. Since a

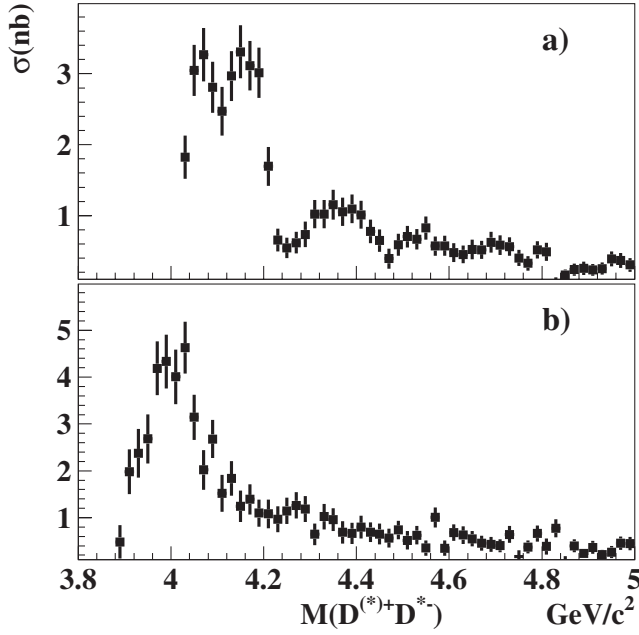


FIG. 2. The exclusive cross sections for (a) $e^+e^- \rightarrow D^{*+}D^{*-}$ and (b) $e^+e^- \rightarrow D^+D^{*-}$.

reliable fit to the cross sections obtained above requires a solution to a nontrivial and model-dependent problem of coupled channels and threshold effects, we do not report results here.

The systematic errors for the $\sigma(e^+e^- \rightarrow D^{(*)+}D^{*-})$ measurements are summarized in Table I. The systematic errors associated with the background (1)–(3) subtraction are estimated to be 3% from the uncertainty in the scaling factors for the sideband subtractions using fits to the $M(D^{(*)+})$ and $\Delta M_{\text{rec}}^{\text{fit}}$ distributions in the data with different signal and background parametrization. Uncertainties in backgrounds (4)–(5) are estimated conservatively to be smaller than 2% of the signal in the case of $D^{*+}D^{*-}$; these two sources are added linearly to give 5% in total. In the case of the D^+D^{*-} , backgrounds (4)–(5) are subtracted using the data and only the uncertainty in the scaling factor for the subtracted distribution is taken into account. A second source of systematic error is due to the unknown helicity angle composition of the $D^{*+}D^{*-}$ final state which

can be a mixture of $D_T^{*+}D_T^{*-}$, $D_T^{*+}D_L^{*-}$ and $D_L^{*+}D_L^{*-}$, where the subscripts L and T refer to longitudinally and transversely polarized D^{*} 's. For the efficiency calculation, we assume equal fractions of these helicity states and consider the extreme cases (pure $D_T^{*+}D_T^{*-}$ and pure $D_L^{*+}D_L^{*-}$) for the efficiency uncertainty. There is no corresponding uncertainty in the case of the D^+D^{*-} final state, where the D^{*-} polarization is fixed by angular momentum and parity conservation. A third source of systematic error comes from the uncertainties in track and photon reconstruction efficiencies, which are 1% per track, 2% per slow pion, and 1.5% per photon, respectively. The systematic error ascribed to the cross-section calculation is estimated from a study of the C dependence of the final result and includes a 1.5% error on the total luminosity. Other contributions come from the uncertainty in the identification efficiency and the absolute D^0 and $D^{(*)+}$ branching fractions [14].

In summary, we report the first measurements of exclusive $e^+e^- \rightarrow D^{*+}D^{*-}$ and $e^+e^- \rightarrow D^+D^{*-}$ cross sections at \sqrt{s} around the $D^{*+}D^{*-}$ and D^+D^{*-} thresholds with initial-state radiation. The shape of the $e^+e^- \rightarrow D^{*+}D^{*-}$ cross section is complicated with several local maxima and minima. The minimum near 4.25 GeV/c^2 —in the $Y(4260)$ region—could be due to $D_s^*D_s^*$ (DD^{**}) threshold effects described in [15–17] or due to destructive interference of this state with other $\psi(nS)$ states. Aside from a prominent excess near the $\psi(4040)$, the $e^+e^- \rightarrow D^+D^{*-}$ cross section is relatively featureless. The measured cross sections are compatible [18] within errors with the $D^{(*)}\bar{D}^*$ exclusive cross section in the energy region up to 4.260 GeV measured by CLEO-c [19].

We thank the KEKB group for excellent operation of the accelerator, the KEK cryogenics group for efficient solenoid operations, and the KEK computer group and the NII for valuable computing and Super-SINET network support. We acknowledge support from MEXT and JSPS (Japan); ARC and DEST (Australia); NSFC and KIP of CAS (China); DST (India); MOERD, KOSEF, and KRF (Korea); KBN (Poland); MIST (Russia); ARRS (Slovenia); SNSF (Switzerland); NSC and MOE (Taiwan); and DOE (U.S.A.).

TABLE I. The systematic errors for cross sections [%].

Source	$D^{*+}D^{*-}$	D^+D^{*-}
Background subtraction	± 5	± 4
Angular distributions	± 5	...
Reconstruction	± 7	± 6
Cross section calculation	± 2	± 2
$\mathcal{B}(D^{(*)})$	± 3	± 5
MC statistics	± 4	± 3
Kaon identification	± 1	± 1
Total	± 11	± 10

- [1] K. K. Seth Phys. Rev. D **72**, 017501 (2005).
- [2] B. Aubert *et al.* (BABAR Collaboration), Phys. Rev. Lett. **95**, 142001 (2005).
- [3] T. E. Coan *et al.* (CLEO Collaboration), Phys. Rev. Lett. **96**, 162003 (2006).
- [4] Q. He *et al.* (CLEO Collaboration), Phys. Rev. D **74**, 091104 (2006).
- [5] K. Abe *et al.* (Belle Collaboration), hep-ex/0612006.
- [6] X. H. Mo *et al.*, Phys. Lett. B **640**, 182 (2006).
- [7] B. Aubert *et al.* (BABAR Collaboration), hep-ex/0607083.
- [8] Charge-conjugate modes are included throughout this Letter.

- [9] A. Abashian *et al.* (Belle Collaboration), Nucl. Instrum. Methods Phys. Res., Sect. A **479**, 117 (2002).
- [10] S. Kurokawa and E. Kikutani, Nucl. Instrum. Methods Phys. Res., Sect. A **499**, 1 (2003), and other papers included in this volume.
- [11] B. Aubert *et al.* (BABAR Collaboration), Phys. Rev. D **70**, 072004 (2004).
- [12] E. Nakano, Nucl. Instrum. Methods Phys. Res., Sect. A **494**, 402 (2002).
- [13] B. Aubert *et al.* (BABAR Collaboration), Phys. Rev. D **73**, 012005 (2006).
- [14] S. Eidelman *et al.* (Particle Data Group), Phys. Lett. B **592**, 1 (2004); also see update at <http://pdg.lbl.gov>.
- [15] M. B. Voloshin, hep-ph/0602233.
- [16] S. Dubynskiy and M. B. Voloshin, Mod. Phys. Lett. A **21**, 2779 (2006).
- [17] J. L. Rosner Phys. Rev. D **74**, 076006 (2006).
- [18] Since only charged final states are measured, our results should be scaled by a factor of 2 for this comparison.
- [19] R. Poling, hep-ex/0606016.